

Citation for published version:
Zhao, K, Ouyang, B, Bowen, CR & Yang, Y 2020, 'Enhanced photocurrent via ferro-pyro-phototronic effect in ferroelectric BaTiO, materials for a self-powered flexible photodetector system', Nano Energy, vol. 77, 105152. https://doi.org/10.1016/j.nanoen.2020.105152

10.1016/j.nanoen.2020.105152

Publication date: 2020

Document Version Peer reviewed version

Link to publication

Publisher Rights CC BY-NC-ND

### **University of Bath**

### **Alternative formats**

If you require this document in an alternative format, please contact: openaccess@bath.ac.uk

**General rights** 

Copyright and moral rights for the publications made accessible in the public portal are retained by the authors and/or other copyright owners and it is a condition of accessing publications that users recognise and abide by the legal requirements associated with these rights.

If you believe that this document breaches copyright please contact us providing details, and we will remove access to the work immediately and investigate your claim.

Download date: 08, Mar. 2023

Enhanced photocurrent via ferro-pyro-phototronic effect in ferroelectric BaTiO3 materials for a self-powered flexible photodetector system

Kun Zhao 1,2, Bangsen Ouyang 1, Chris R. Bowen3, and Ya Yang 1,4,5\*

<sup>1</sup>CAS Center for Excellence in Nanoscience, Beijing Key Laboratory of Micro-nano Energy and Sensor, Beijing Institute of Nanoenergy and Nanosystems, Chinese Academy of Sciences, Beijing 100083, P. R. China.

<sup>2</sup>State Key Laboratory of Advanced Processing and Recycling of Nonferrous Metals, School of Materials Science and Engineering, Lanzhou University of Technology, Lanzhou 730050, China Department of <sup>3</sup>Mechanical Engineering, University of Bath, BA2 7AK, UK

<sup>4</sup>School of Nanoscience and Technology, University of Chinese Academy of Sciences, Beijing, 100049, P. R. China.

<sup>5</sup>Center on Nanoenergy Research, School of Physical Science and Technology, Guangxi University, Nanning 530004, PR China.

Ferroelectric materials have demonstrated excellent photovoltaic effects in order to scavenge light energy under illumination. However, the ability to achieve simultaneously both a high photocurrent and output voltage from ferroelectric materials remains a challenge. Herein, a ferroelectric BaTiO<sub>3</sub>-based photovoltaic-pyroelectric coupled effect flexible photodetector system is presented to detect light and heat simultaneously and significantly boost their photocurrent. The devices offer a low cost and scalable route for directly converting light and heat into electricity while being able to operate without the need for any external power source. As compared with photovoltaic effect, the corresponding coupled current peak and plateau were 451.9 % and 17.2 % higher than under light alone due to the photovoltaic-pyroelectric coupled effect, respectively. The enhanced performance can be explained by a photovoltaic-pyroelectric coupled effect with induced energy band bending. As a demonstration of its application, we designed a self-powered flexible photodetector system that is suitable for detecting and recognizing light intensities and temperature variations by recording the electrical signals as a mapping figure.

**KEYWORDS**: BaTiO<sub>3</sub>, Photodetector systems, photovoltaic-pyroelectric coupled effect, self-powered.

With the urgent demand for clean and sustainable new energy, it is critical to develop low power micro/nano sensors and self-powered nano devices 1-6. For this reason, a variety of devices have been explored based on the photovoltaic effect<sup>7-9</sup>, pyroelectric effect<sup>10-12</sup>, thermoelectricity<sup>13-15</sup> and piezoelectricity<sup>16-18</sup> in order to directly convert light energy, temperature differences, thermal energy and pressure into electrical energy. Significantly, ferroelectric materials, such as BiFeO<sub>3</sub> (BFO) <sup>19-21</sup>, Pb(Zr,Ti)O<sub>3</sub> (PZT) <sup>22,23</sup>, BaTiO<sub>3</sub> (BTO) <sup>24-26</sup>, and LiNbO<sub>3</sub><sup>27-29</sup> have been reported to make important progress in heat, light, and pressure detection in recent years. However, the majority of such devices can only convert a single source of energy into electrical energy, resulting in more expensive and the lower power conversion efficiencies, which has greatly influenced and limited a wide application in many fields such as public security, wearables, robotics and internet of things. Thus, it is necessary to develop multifunctional devices that are able to harvest multiple sources of energy simultaneously. Our group has investigated BTO material devices under light illumination due to photovoltaic-pyroelectric coupled effect<sup>30</sup> and conjuncted pyro-piezoelectric effect<sup>31</sup> for self-powered simultaneous temperature and pressure sensing. However, there has been no reports to date on the enhancement of the photocurrent in BTO materials by photovoltaic-pyroelectric coupled effect for self-powered flexible photodetector systems. Such devices are of interest to detect light and environmental temperature changes for simultaneous multi-signal sensing and exploit light-temperature coupled electricity.

Herein, we present a self-powered flexible photodetector system based on photovoltaic-pyroelectric coupled effect using a ferroelectric BTO ceramic sheet as the sensor unit for detector the 405 nm light intensity and temperature without using external power source. A BTO ceramic sheet with the lightfacing side of indium tin oxide (ITO) electrode and the other side is Ag electrode. A soft kapton membrane allows the device to be flexible and integrated, providing potential applications in the field of wearable electronics, environmental sensors and artificial intelligent sensors. The system not only can be used to detect individual sources light and temperature accurately, but is able to respond to light and temperature simultaneously. The output voltage of 16 ITO/BTO/Ag sensing units were simultaneously recorded as a mapping image in real time. Under a light intensity of 7.78 mW/cm<sup>2</sup> and a heating temperature of 22.1 K, the photodetector is able to generate a coupled current peak was 451.85 % higher than by illumination alone due to the photovoltaic-pyroelectric coupled effect. In addition, under a light intensity of 7.78 mW/cm<sup>2</sup> and a cooling temperature of -14.5 K, the photodetector can generate a coupled stable current plateau that is enhanced by 17.16 % after utilizing a cooling temperature variation. Moreover, the output voltage signals of 4×4 matrix of ITO/BTO/Ag device array were simultaneously recorded in real time as a mapping figure. The single source or coupled information can be determined by analyzing the self-generated electric signals and this novel form of self-powered flexible photodetector system provide new approaches for rapid and accurate detection of light-temperature coupled signals.

A schematic of the fabricated ITO/BTO/Ag photodetector under simultaneous light illumination and temperature variation is shown in Fig. 1a, which consists of an upper transparent ITO electrode, a BTO ceramic sheet and a lower Ag electrode. Fig. 1b presents BTO particles with a diameter of approximately 50-100 nm prior to sintering, and the corresponding scanning electron microscopy (SEM) image at low magnification is shown in Supplementary Fig. 1a. After sintering processing at 1200 °C, the X-ray diffraction patterns (Supplementary Fig. 1b) indicate that the BTO ceramic sheets have an orthorhombic phase, which provides the materials with a spontaneous polarisation. The surface and cross-sectional SEM images of BTO ceramic sheets shows that the average grain size of the sample was 140-400 nm and the structure of specimen was compact and dense; see Supplementary Fig. 1c-1f. Figs. 1c and 1d show a photograph and SEM image of the fabricated devices which acts as the base unit for the self-powered flexible photodetector system, having a diameter of approximately 8 mm and a thickness of ~200  $\mu$ m, respectively. The measured piezoelectric coefficient  $d_{33}$  of fabricated device was 310 pC/N after poling by applying an electric field of 2.3 kV/mm in a silicone oil bath at room temperature.

Fig. 2a shows the output current signals of the device under 405 nm illumination with different light intensities, where the current peaks and current plateaus signals can be increased from 5.4 to 43.2 nA and from 5 to 40 nA on increasing the light intensity from 7.78 to 127.6 mW/cm<sup>2</sup>, respectively. As depicted in Fig. 2b, a sharp current peak followed by a stable plateau can be seen under simultaneous light illumination and heating temperature variation. The current peaks and current plateaus signals of photovoltaic-pyroelectric effect coupled can be increased from 29.8 to 69.7 nA and from 4.46 to 35 nA on increasing the light intensity from 7.78 to 127.6 mW/cm<sup>2</sup> and temperature variations with a heating temperature change of  $\Delta T = 22.1$  K, respectively. Compared with Figs. 2a and 2b, it can be seen that the current peak and current plateau signals from the photovoltaic-pyroelectric coupled effect increases with increasing light intensity, but the current plateau is smaller compared to conditions of individual light illumination. In addition, the output current signal of the device under simultaneous light illumination with intensities ranging from 7.78 mW/cm<sup>2</sup> to 127.6 mW/cm<sup>2</sup> and a cooling temperature change of  $\Delta T =$ -14.5 K are illustrated in Fig. 2c. The current peak signal due to the photovoltaic-pyroelectric effect coupling decreases from -19.2 to -12 nA but the current plateau signals are increased from 5.9 to 44.9 nA on increasing the light intensity from 7.78 to 127.6 mW/cm<sup>2</sup> at the same cooling temperature variations. The result indicates that the current plateau signals can be dramatically enhanced by use of a cooling temperature variation. Figs. 2d and 2e displays the change of photocurrent peak signals/signal enhancement ratio and photocurrent plateau signals/signal enhancement ratio under different conditions, respectively. These results show that a heating temperature variation can be used to enhance the output current peak signal and a cooling temperature variation can be utilized to increase the current plateau signal of the fabricated ITO/BTO/Ag device. Under a light intensity of 7.78 mW/cm<sup>2</sup>, the device under simultaneous 405 nm light illumination and a heating temperature variation ( $\Delta T = 22.1 \text{ K}$ ) can generate

a coupled photocurrent peak that was 451.85 % higher than light alone due to the photovoltaic-pyroelectric coupled effect (Fig. 2d). Interestingly, the output coupled photocurrent plateau of the device can be enhanced by 17.16 % by utilizing a cooling temperature variation ( $\Delta T$ =-14.5 K) when compared with the photocurrent of the device under individual light illumination (7.78 mW/cm²). It is worth noting that the enhancement ratios of the photocurrent decrease with increasing light intensity. The corresponding output voltage signals and enhancement ratios of the devices under individual 405 nm light illumination and simultaneous light-temperature variation also follow a similar pattern, as seen in Supplementary Fig. 8.

To confirm that the output electrical signals of the device are caused by the photovoltaic or pyroelectric effects, the output voltage and current signals were measured under individual periodically light illumination and heating and cooling conditions, see Supplementary Fig. 2. Under a forward connection, a positive voltage/current signals were observed under a 405 nm light intensity of 127.6 mW/cm<sup>2</sup> (Supplementary Figs. 2a and 2b). By reversely connecting the device to the measured system, opposing polarity voltage/current signals were observed under the same light intensity (Supplementary Figs. 2c and 2d). In addition, the voltage/current signals of the device were observed to periodically change under cooling ( $\Delta T$ =-14.5 K) (Supplementary Figs. 2e and 2f) and heating ( $\Delta T$ =22.1 K) conditions, as seen in Supplementary Figs. 2g and 2h. The relevant mechanism of the fabricated ITO/BTO/Ag device is based on the thermally induced random oscillation of the dielectric dipoles around its equilibrium axis at room temperature (Supplementary Fig. 3a). On heating, the temperature of the device increases and the random oscillation state of the dielectric dipoles at room temperature is disturbed, resulting in greater oscillation to a larger degree around their respective symmetry axes and the total average spontaneous polarization is decreased and the induced charges at the electrode are reduced, resulting in a flow of electrons from the ITO electric to the Ag electrode (Supplementary Fig. 3b). Thus, a positive pyroelectric voltage/current is observed (Supplementary Figs. 2e and 2f). Under cooling conditions, the dielectric dipoles oscillate to a smaller degree around their respective symmetry axes and the corresponding spontaneous polarization is increased, resulting in a flow of electrons from the Ag electrode to the ITO electrode (Supplementary Fig. 3c). Therefore, a negative pyroelectric voltage/current is observed (Supplementary Figs. 2g and 2h). Based on the pyroelectric effect, the pyroelectric performance of the polarized BTO device are illustrated in Supplementary Fig. 4-6. The periodic heating conditions from 3.0 to 22.1 K in Supplementary Fig. 4a are applied using a semiconductor heater. The positive voltage/current peak signals can be increased from 0.13 to 0.79 V/ 3.8 to 25.1 nA which correspond to heating variations shown in Supplementary Fig. 4b and Supplementary Fig. 6a, respectively. In addition, the periodic cooling conditions from -2.4 to -14.5 K in Supplementary Fig. 5a are applied by using a semiconductor cooler. The negative voltage/current peak signals are increased from -0.11 to -0.67 V/ -3.9 to -22.3 nA, which correspond to the cooling variations displayed in<sub>4</sub>

Supplementary Fig. 5b and Supplementary Fig. 6c, respectively. Supplementary Fig. 6b presents infrared images of the device surface in the different heating (top) and cooling (bottom) temperatures. The calculated charge densities and pyroelectric coefficients ( $P_c$ ) of different temperature variations of the ITO/BTO/Ag device are shown in Fig. S6d and S6e. As a result of the increased temperature variations in device, the calculated charge densities are gradually enhanced. When the heating temperature increased from 3.0 to 22.1 K, the charge density increases from 63.4 to 513.5 nC/cm², and the cooling temperature increased from -2.4 to -14.5 K, the charge density increases from -68.4 to -577.3 nC/cm². The corresponding pyroelectric coefficients of the device can be calculated to be approximately13-19 nC/cm²K (heating) and 22-42 nC/cm²K (cooling), respectively.

To evaluate the sensitivity of device to 405 nm light illumination, the photoconductive gain (G), responsivity (R) and specific detectivity ( $D^*$ ) were calculated from Supplementary Figs. 7a and 7b. The  $G_2$ ,  $R_2$  and  $D^*_2$  derived from photovoltaic-pyroelectric coupled effect showed larger values than  $G_1$ ,  $R_1$  and  $D^*_1$  that obtained from photovoltaic effect, which were initially quickly increased and then became stable with increasing 405nm light intensity. However,  $G_1$ ,  $R_1$  and  $D^*_1$  exhibited a decreasing tendency with increasing light intensity. Under light illumination of 7.78 mW/cm², the values of  $G_2$ ,  $R_2$  and  $D^*_2$  were approximately 5.5 times larger than  $G_1$ ,  $R_1$  and  $D^*_1$ . Moreover, under light illumination of 126.7 mW/cm², the values of  $G_2$ ,  $R_2$  and  $D^*_2$  were approximately 1.6 times larger than  $G_1$ ,  $R_1$  and  $D^*_1$ . We also investigated the response time of the device to 405 nm light illumination of 127.6 mW/cm² (Supplementary Figs. 7c and 7d), which clearly shows that the device exhibits a good photo-response component with a rise time of 0.88 s and a fall time of 1.06 s, where the time was calculated between 10 % and 90 % of the output photocurrent signal when the light was turned on and off, respectively.

Fig. 3a shows a schematic of the device's voltage measurement with a 100 M $\Omega$  loading resistance. To further clarify the effect of photovoltaic-pyroelectric coupled effect on the output electrical signals, we measured the photovoltage signals of the device under individual light illumination (127.6 mW/cm²), heating ( $\Delta T$ =22.1 K), and simultaneous light-heating states, as displayed in Fig. 3b. It can be seen that the photovoltage under conditions of simultaneous light-heating is not a simple superposition of the photovoltage signals under individual light and heating conditions. When compared with individual light illumination, the photovoltage plateau can be decreased due to the coupling of light and heating. When compared with individual light (127.6 mW/cm²) and cooling ( $\Delta T$ =-14.5 K) conditions, the coupling enhancement of the photovoltage plateau can be clearly observed under the simultaneous application of light and cooling on the device, as illustrated in Fig. 3c. The corresponding photocurrent signals and photovoltage/photocurrent signals under different light intensities from 127.6 to 7.78 mW/cm² on the device exhibit a similar change (Supplementary Fig. 9-12). Supplementary Fig. 13 presents a comparison of the measured output voltage plateau (Supplementary Fig. 13a) and current plateau (Supplementary Fig. 13b) under the different light illumination intensities due to the photovoltaic-pyroelectric coupled5

effect (Supplementary Fig. 9-12). We found that the photovoltage plateau can be increased from 0.16 to 0.76 V when the light intensity increased from 7.78 to 127.6 mW/cm<sup>2</sup>. The light-heating coupled photovoltage plateau can be increased from 0.14 to 0.52 V and light-cooling coupled photovoltage plateau can be increased from 0.19 to 0.92 V, respectively (Supplementary Fig. 13a). Under the same light intensity, the corresponding photocurrent plateau signals of the device shows the decreasing order among light-cooling, individual light and light-heating. This behavior for the enhancement of photocurrent plateau in Supplementary Figure 11b can be understood due to the photovoltaic-pyroelectric coupled effect on the energy band structures of the device, as depicted in Supplementary Fig. 3d-3g. The device has a ITO/BTO/Ag structure, which can be regarded as a BTO layer sandwiched between two back-to-back Schottky barriers each interface. After the BTO layer was polarized, the negative and positive polarized charges can increase and decrease the Schottky barrier height at the BTO/ITO and BTO/Ag interfaces, respectively. As shown in Fig. 3e, the 405 nm illumination-induced electron and hole pairs can be effectively separated by the left Schottky barrier to produce the photocurrent signals that are detected. When the device is subjected to combined light and heating, the polarized charges of the BTO layer are decreased, resulting in a reduction of the left Schottky barrier height. Moreover, the right Schottky barrier height is increased due to the decrease of positive polarized charges in the BTO, as shown in Fig. 3f. The reduction of the left Schottky barrier height acts to weaken the effective separation of light-induced electron-hole pairs, and the increased Schottky barrier height at the right interface is detrimental to the flow of electrons from BTO to the right Ag electrode, resulting in the decrease of the photocurrent plateau. However, when the device is combined light and cooling, the polarized charges of BTO layer are increased, resulting in an increase of the left Schottky barrier height, which is more effective to separate the light-induced electronhole pairs. Meanwhile, a decrease of the right Schottky barrier height will act to promote the flow of electrons from BTO to the right Ag electrode. Therefore, the photocurrent plateau can be effectively enhanced by the coupling of both light and cooling in the device.

To better research the potential application of signal ITO/BTO/Ag device, a self-powered flexible photodetector systems was designed by using a 4×4 photovoltaic-pyroelectric sensing matrix of ITO/BTO/Ag devices and a kapton film, the 4×4 ITO/BTO/Ag arrays attached to the kapton film were integrated together and were flexible, as illustrated in Fig. 4a-4c and Supplementary Fig. 15. The flexible photodetector system is able to bend at different radians to adapt to the changing testing position (Figs. 4b and 4c). More importantly, 16 units with two Cu wires each one was connected to a multichannel data acquisition system to collect real-time sensing data. The voltage-time curves of 16 channels induced by the 405 nm light (127.6 mW/cm²) are demonstrated in Fig. 4d. The record voltage plateau range is 0.58-0.77 V, indicating that each unit of the photodetector system has good stability and presented similar voltage signal as the light on/off. Moreover, Fig. 4e and Supplementary Fig. 16 displays the V-t curves<sub>6</sub>

when 405 nm light illumination was applied on 4×4 ITO/BTO/Ag arrays through a mask with a "N" (Fig. 4e), "U" and "O" shape on it. The corresponding mapping images are presented in Supplementary Fig. 17. The results show that the channels that receive light have normal output voltage signals, while the blocked channels do not detect signals. In addition, each unit of the photodetector systems shows good pyroelectric properties, see Supplementary Fig. 18, and photovoltaic-pyroelectric coupled properties, Supplementary Fig. 19, where the output voltage of each ITO/BTO/Ag unit increases with increasing light intensity from 31.7 to 127.6 mW/cm² (mask with "N") and the output voltage exhibits a linear relationship with the light intensity. In addition, the output signal of each ITO/BTO/Ag unit is independent, and no interference was observed from neighboring units, indicating the dependability of the flexible photodetector systems (Supplementary Fig. 20).

Fig. 5 illustrates the output voltages and the mapping images of photodetector system using a mask with "N" shape on it under 'no light', 'light only', 'light + heating' and 'light + cooling' conditions. As shown in Fig.5a and 5c, the channels with an open area record photovoltaic-pyroelectric coupled signals, but the sheltered channels only exhibit a pyroelectric response. According to the four conditions, the voltage-curves and mapping images of the self-powered flexible photodetector systems can be divided into four stages as follows: In the stage I, all the ITO/BTO/Ag units show green color in the mapping figure with no light applied, corresponding to the blue line labelled "I" in Fig. 5a where no output signals were observed. In the stage II, on illuminating the device with light, a clear color change was observed on the non-masked areas, while the masked areas maintained the same green color. Under simultaneous light illumination and heating temperature variation conditions, the lowest voltage plateau is obtained in the non-masked channels (stage III). While the highest voltage plateau is recorded in non-masked channels of the photodetector system under simultaneous illumination by light and accoling temperature variation conditions (stage IV). The result indicate the voltage plateau of system under individual light (II) higher the light + heating (III) and lower light + cooling (IV) conditions. Moreover, the designed self-powered flexible photodetector system has good stability and repeatability under different conditions, as illustrated in Supplementary Fig. 21-24.

In conclusion, our findings demonstrate a novel photovoltaic-pyroelectric simultaneous sensing system using highly responsive ferroelectric BTO sheets. Under light illumination and cooling simultaneous, the fabricated flexible photodetector system delivers an enhancement of current/voltage plateau signals due to a photovoltaic-pyroelectric coupled effect. The corresponding photoconductive gain, responsivity and specific detectivity of the photodetector can be enhanced by over 160 % at a light intensity of 127.6 mW/cm² as compared with that by utilizing photovoltaic effect. A 4×4 matrix of self-powered photodetector system has been utilized to achieve ambient light illumination and temperature variations detection by real-time recording the output voltage signals of 16 ITO/BTO/Ag units as a mapping figure. The ferroelectric BTO materials with photovoltaic-pyroelectric coupled effect present a<sub>7</sub>

great potential application for future technologies such as wearable electronics, environmental sensors and artificial intelligent sensors.

### References

- 1. Wang, Z. L. On Maxwell's displacement current for energy and sensors: the origin of nanogenerators. *Materials Today* **20**, 74-82 (2017).
- 2. Zhang, C. et al. Active micro-actuators for optical modulation based on a planar sliding triboelectric nanogenerator. *Adv. Mater.* **27**, 719-726 (2015).
- 3. Fan, F. R., Tang, W., Wang, Z. L. Flexible nanogenerators for energy harvesting and self-powered electronics. *Adv. Mater.* **28**, 4283-4305 (2016).
- 4. Feng, J. et al. Single-layer MoS<sub>2</sub> nanopores as nanopower generators. *Nature* **536**, 197-200 (2016).
- 5. Lee, J. et al. Micropatterned P(VDF-TrFE) film-based piezoelectric nanogenerators for highly sensitive self-powered pressure sensors. *Adv. Funct. Mater.* **25**, 3203-3209 (2015).
- 6. Wang, Z. et al. Light-induced pyroelectric effect as an effective approach for ultrafast ultraviolet nanosensing. *Nat. Commun.* **6**, 8401 (2015).
- 7. Ji, T. et al. An interface engineered multicolor photodetector based on n-Si(111)/TiO<sub>2</sub> nanorod array teterojunction. *Adv. Funct. Mater.* **26,** 1400-1410 (2016)
- 8. Krishnamoorthy, T. et al. Lead-free germanium iodide perovskite materials for photovoltaic applications. *J. Mater. Chem. A* **3,** 23829-23832 (2015).
- 9. Xiao, Z. et al. Giant switchable photovoltaic effect in organometal trihalide perovskite devices. *Nat. Mater.* **14**, 193-198 (2015).
- 10. Esin, A. et al. Pyroelectric effect and polarization instability in self-assembled diphenylalanine microtubes. *Appl. Phys. Lett.* **109**, 142902 (2016).
- 11. Ma, N., Yang, Y. Enhanced self-powered UV photoresponse of ferroelectric BaTiO<sub>3</sub> materials by pyroelectric effect. *Nano Energy* **40**, 352-359 (2017).
- 12. Wang, X. et al. Light-triggered pyroelectric nanogenerator based on a pn-junction for self-powered near infrared photosensing. *ACS Nano* **11**, 8339-8345 (2017).
- 13. Zhang, F. et al. Flexible and self-powered temperature–pressure dual-parameter sensors using microstructure-frame-supported organic thermoelectric materials. *Nat. Commun.* **6,** 8356 (2015).
- 14. Champier, D. et al. Thermoelectric generators: A review of applications. *Energ. Convers. Manage*. **140**, 167-181 (2017).
- 15. Bahk, J. et al. Flexible thermoelectric materials and device optimization for wearable energy harvesting. *J. Mater. Chem. C* **3**, 10362-10374 (2015).

- 16. Zhu, H. et al. Observation of piezoelectricity in free-standing monolayer MoS<sub>2</sub>. *Nat. Nanotechnol.* **10**, 151-155 (2015).
- 17. Li, F. et al. Ultrahigh piezoelectricity in ferroelectric ceramics by design. *Nat. Mater.* **17**, 349-354 (2018).
- 18. Rodrigues, G. d. C. et al. Strong piezoelectricity in single-layer graphene deposited on SiO<sub>2</sub> grating substrates. *Nat. Commun.* **6**, 7572 (2015).
- 19. You, L. et al. Enhancing ferroelectric photovoltaic effect by polar order engineering. *Sci. Adv.* **4**, eaat3438 (2018).
- 20. Rojac, T. et al. Domain-wall conduction in ferroelectric BiFeO<sub>3</sub> controlled by accumulation of charged defects. *Nat. Mater.* **16**, 322-327 (2017).
- 21. Choi, T. *et al.* Switchable ferroelectric diode and photovoltaic effect in BiFeO<sub>3</sub>. *Science* **324**, 63-66 (2009).
- 22. Yang, Y. et al. Pyroelectric nanogenerators for driving wireless sensors. *Nano Lett.* **12**, 6408-6413 (2012).
- 23. Yang, X. et al. Enhancement of photocurrent in ferroelectric films via the incorporation of narrow bandgap nanoparticles. *Adv. Mater.* **24**, 1202-1208 (2012).
- 24. Zhao, K., Ouyang, B. & Yang, Y. Enhancing photocurrent of radially polarized ferroelectric BaTiO<sub>3</sub> materials by ferro-pyro-phototronic effect. *iScience*, **3**, 208-216 (2018).
- 25. Wu, L. et al. Infrared-to-ultraviolet light-absorbing BaTiO3-based ferroelectric photovoltaic materials. *J. Am. Ceram. Soc*, **102**, 4188-4199 (2019).
- 26. Ma, N., Yang, Y. Boosted photocurrent in ferroelectric BaTiO3 materials via two dimensional planar-structured contact configurations. *Nano Energy* **50**, 417-424 (2018).
- 27. Glass, A. M., Von der Linde, D. & Negran T. J. High-voltage bulk photovoltaic effect and the photorefractive process in LiNbO<sub>3</sub>. *Appl. Phys. Lett.* **25**, 233-235 (1974).
- 28. Arizmendi, L. Photonic applications of lithium niobate crystals. *Phys. Status Solidi A* **201**, 253-283 (2004).
- 29. Carnicero, J. *et al.* Superlinear photovoltaic currents in LiNbO<sub>3</sub>: analyses under the two-center model. *Appl. Phys.* B **79**, 351-358 (2004).
- 30. Ma, N. Zhang, K. & Yang, Y. Photovoltaic-pyroelectric coupled effect induced electricity for self-powered photodetector system. *Adv. Mater.* **29,** 1703694 (2017).
- 31. Song, K. et al. Conjuncted pyro-piezoelectric effect for self-powered simultaneous temperature and pressure sensing. *Adv. Mater.*, 1902831 (2019).

## Acknowledgments

This work was supported by the National Key R&D Program of China (Grant No. 2016YFA0202701), the National Natural Science Foundation of China (Grant Nos. 51472055), External Cooperation Program of BIC, Chinese Academy of Sciences (Grant No. 121411KYS820150028), the 2015 Annual Beijing Talents Fund (Grant No. 2015000021223ZK32), Qingdao National Laboratory for Marine Science and Technology (No. 2017ASKJ01), the University of Chinese Academy of Sciences (Grant No. Y8540XX2D2), and the "thousands talents" program for the pioneer researcher and his innovation team, China.

#### **Author contributions**

Y. Y. conceived and supervised the research. K. Z. and B. O. carried out the device fabrication and the performance measurement, K. Z., B. O., C. B. and Y. Y. analyzed the data and co-wrote the manuscript.

### **Competing interests**

The authors declare no competing financial interests.

### **Additional information**

Supplementary Information is available in the online version of the paper. Reprints and permissions information is available online at www.nature.com/reprints. Correspondence and requests for materials should be addressed to Y. Y.

### Methods

**Preparation of BTO ceramic sheets.** Several drops of PVA-water solution (2 wt. %) were completely mixed with 0.3g BTO nanoparticles. Then, the obtained fine powder was transferred to a stainless steel mould with a diameter of 10 mm, and it was pressed into disks of 10 mm in diameter under a pressure of 2.5 MPa with a powder compression machine. Afterwards, BTO sheets were sintered at 650 °C for 1 h to eliminate the PVA binder and then sintered at 1200 °C for 2 h in a muffle furnace.

**Fabrication of the devices.** Initially, a thin layer of Ag electrode was sputtered on the two surfaces of the prepared BTO ceramic sheets by a magnetron sputtering system (Beijing jinshengweina technology Co. MSP-820). Then, the Ag/BTO/Ag devices were poled for 30 min under an applied electric field of 2.3 kV/mm in silicone oil bath at room temperature. Finally, by removing one Ag electrode and polishing the BTO ceramic sheet to a thickness of ~200  $\mu$ m, an ITO electrode was deposited on the polished side by RF magnetron sputtering for 15 min under power of 150 W. The 4×4 matrix flexible photodetector system was constructed by a 16 ITO/BTO/Ag devices and a piece of  $50 \times 50 \times 0.03$  mm kapton membrane.

Characterizations and Measurements. SEM images were obtained using a field-emission scanning electron microscope (Hitachi SU8020). The crystal structure of BTO nanoparticles was identified by an X-ray diffractometer (Panalytical X'pert<sup>3</sup> powder), using Cu K $\alpha$  radiation. The temperature was measured by infrared thermometer (Optris PI400). The output voltage and current signals of the devices were measured by a low-noise preamplifier (Stanford Research SR560) and a low-noise current preamplifier (Stanford Research SR570), respectively. The output voltage signals of the  $4\times4$  matrix of ITO/BTO/Ag device array were measured by a multichannel data acquisition system (National Instruments NI PXle-1082).

## **Data availability**

The data that support the plots within this paper and other finding of this study are available from the corresponding author upon reasonable request.

# **FIGURES**

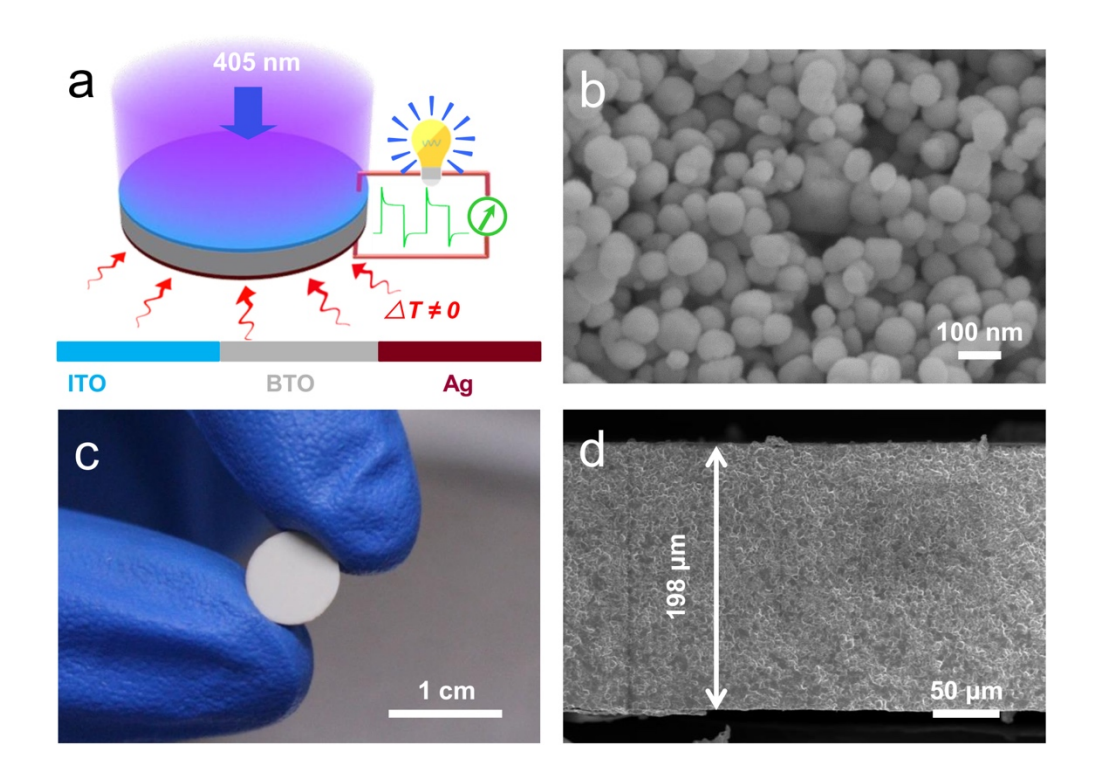


Fig.1 | Characterization of the ITO/BTO/Ag photodetector. a, Schematic of the fabricated device. b, SEM image of the BTO particles. c, Photograph of a single ITO/BTO/Ag device. d, Thickness of the fabricated device observed by SEM.

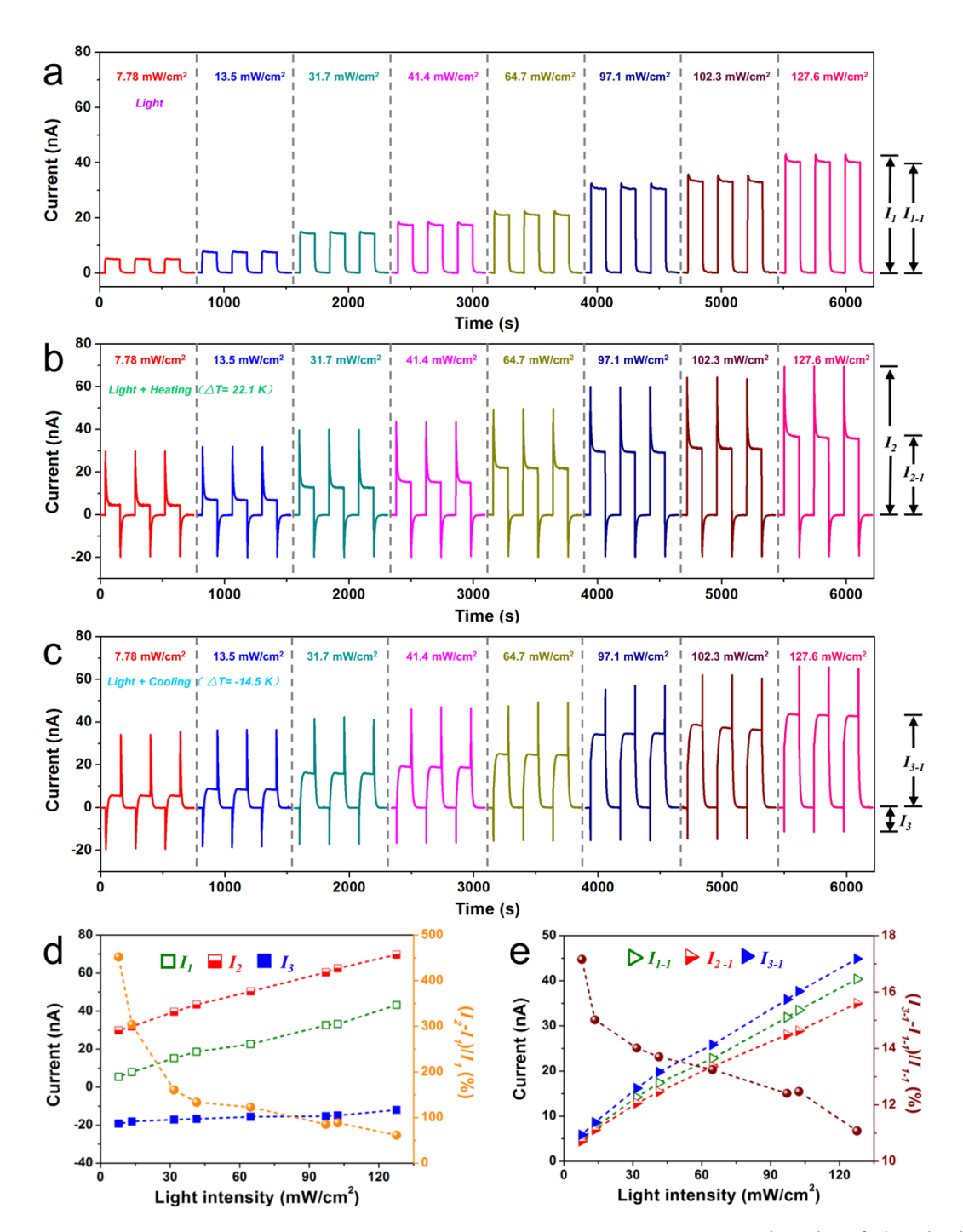


Fig.2 | Performance of ITO/BTO/Ag photodetector. a, Output current signals of the device under 405 nm illumination with light intensities ranging from 7.78 mW/cm<sup>2</sup> to 127.6 mW/cm<sup>2</sup>. b,c, Output current signals of the device under simultaneous light illumination with intensities ranging from 7.78 mW/cm<sup>2</sup> to 127.6 mW/cm<sup>2</sup> and temperature variations with a heating temperature change of  $\Delta T = 22.1$  K (b) and a cooling temperature change of  $\Delta T = -14.5$  K (c). d, Comparison of the measured output current peak and current peak enhanced ratios of the devices under the different light illumination intensities due to the photovoltaic-pyroelectric coupled effect; e, Comparison of the measured output current plateau and plateau enhanced ratios of the devices under the different light illumination intensities due to the photovoltaic-pyroelectric coupled effect.

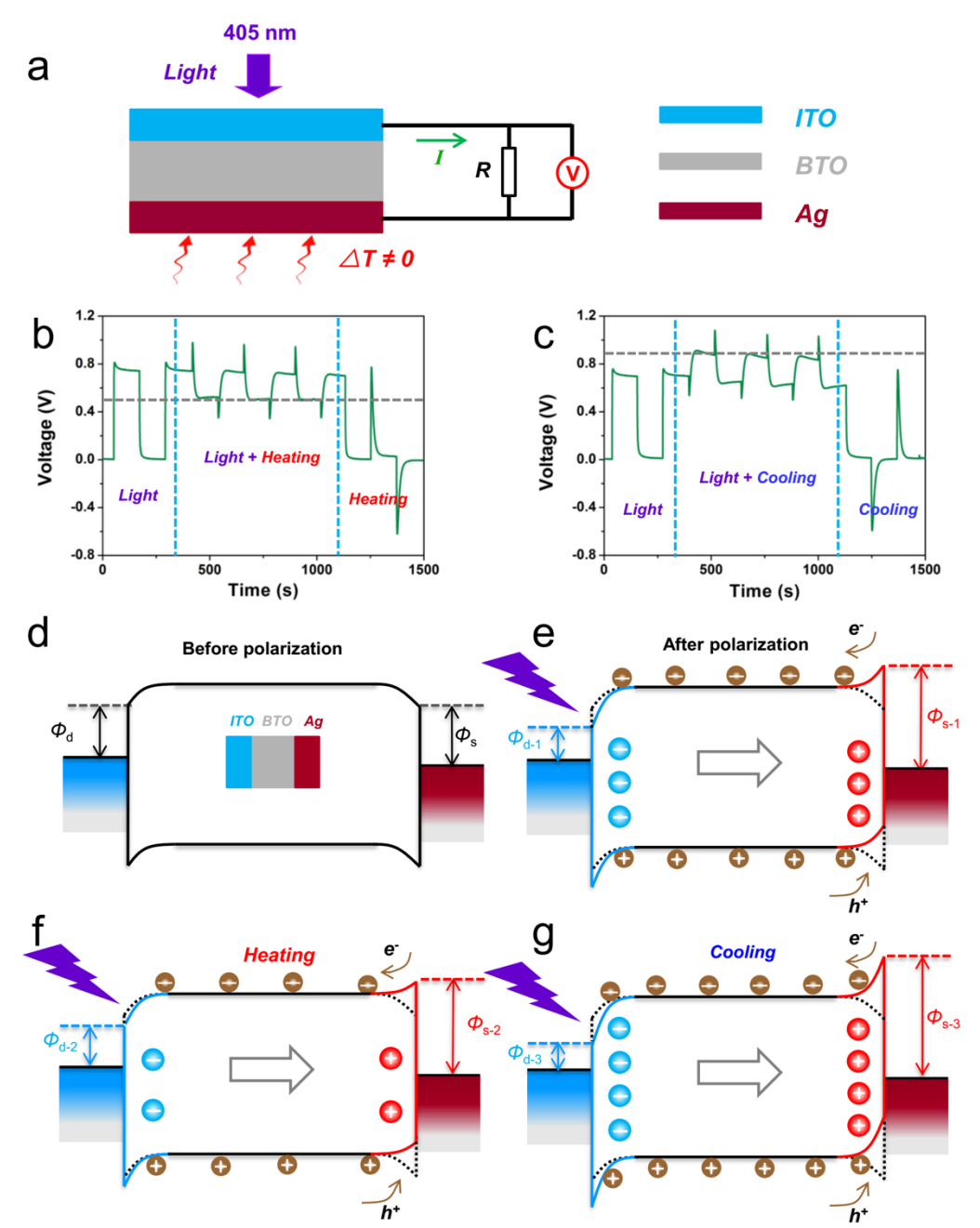


Fig.3 | Schematic diagram, measured voltage signals under photovoltaic-pyroelectric coupled effect and energy band structures of the device. a, Schematic of the device's voltage measurement. b, Measured output voltage signals of the device under the individual 405 nm light illumination (127.6 mW/cm²), simultaneous light illumination and temperature variations with a heating temperature change of  $\Delta T = 22.1$  K and the individual heating conditions. c, Measured output voltage signals of the device under the individual 405 nm light illumination (127.6 mW/cm²), simultaneous light illumination and temperature variations with a cooling temperature change of  $\Delta T = -14.5$  K and the individual cooling conditions. d-g, Schematics of the energy band structures of the device: (d) Before polarization. (e) Under 405 nm light illumination after polarization of the device. (g) Under simultaneous 405 nm light illumination and heating conditions after polarization of the device. (g) Under simultaneous 405 nm light illumination and cooling conditions after polarization of the device.

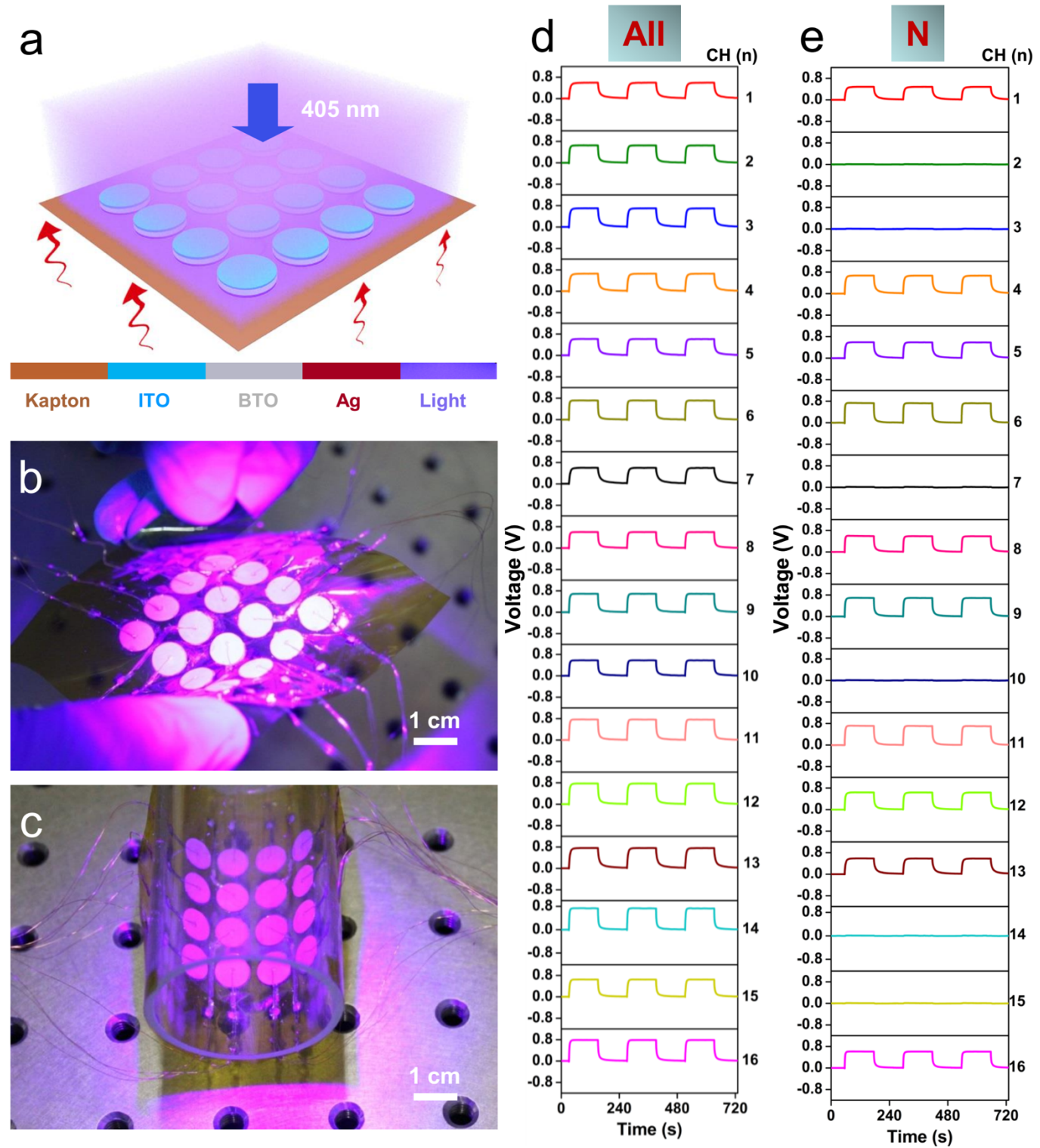


Fig.4 | ITO/BTO/Ag device array as self-powered flexible photodetector system and output V-t curves under 405nm light illumination. a, Schematic of the fabricated 4×4 matrix of ITO/BTO/Ag photodetector system. b, Photograph showing the self-powered flexible photodetector system under 405 nm light illumination in the bent state. c, Photograph of the self-powered flexible photodetector system attached on a cylindrical acrylic pipe under 405 nm light illumination to demonstrate flexibility. d,e, Voltage-time curves of the self-powered photodetector system under 405 nm light illumination (127.6 mW/cm²) through all channel (d) and a letter of "N" (e).